We are IntechOpen,
the world's leading publisher of
Open Access books
Built by scientists, for scientists

4,800
Open access books available

122,000
International authors and editors

135M
Downloads

154
Countries delivered to

Our authors are among the

TOP 1%
most cited scientists

12.2%
Contributors from top 500 universities

CLARIVATE ANALYTICS
BOOK CITATION INDEX
INDEXED

WEB OF SCIENCE™

Selection of our books indexed in the Book Citation Index
in Web of Science™ Core Collection (BKCI)

Interested in publishing with us?
Contact book.department@intechopen.com

Numbers displayed above are based on latest data collected.
For more information visit www.intechopen.com

Kinetic Modelling in Human Brain Imaging

Natalie Nelissen[1], James Warwick[2] and Patrick Dupont[1]
[1]*K.U.Leuven*
[2]*Stellenbosch University*
[1]*Belgium*
[2]*South Africa*

1. Introduction

Kinetic modelling is an important tool in Positron Emission Tomography (PET) which enables us to study the kinetics of tracers. Two important applications of this technique are its use in drug development and in the study of the neurochemistry of the brain. A major issue that we encounter when using kinetic modelling is the selection of the model and understanding its limits and pitfalls. Furthermore, the acquisition, reconstruction and processing of PET data also affects the kinetic modelling thereof. Therefore, we define the following three main objectives for the reader of this chapter:

- To understand how the acquisition, reconstruction and processing of data affects its kinetic modelling.
- To understand the rationale, the limits and the pitfalls of each model.
- To understand how model selection can be performed.

2. Acquisition

The acquisition process can be roughly divided into four different parts:

1. Preparation and monitoring of the patient
2. Injection of the tracer
3. PET measurement
4. Sampling of blood (optional)

2.1 Preparation and monitoring of the patient

Most studies for quantification of tracer kinetics last for a relatively long time (typically 60-90 minutes). Therefore, it is important to pay attention to the comfort of the patient when he or she is positioned in the scanner as well as to use elements which can reduce head movement (e.g. a tape around the head to fixate it). Due to the optimal performance at the centre of the scanner, the head needs to be positioned in the central part of the field of view. If needed, monitoring can be performed during the acquisition (e.g. ECG or blood pressure). When the EEG needs to be monitored, this gives rise to local hot spots at the location of the electrodes and introduces a small positive quantification bias in the reconstructed image in voxels located in the brain (Lemmens et al. (2008)). This is caused by metal artifacts from the CT used for

attenuation correction. Algorithms for metal artifact reduction in CT can be used to reduce this problem (De Man et al. (2000)).

It is noteworthy to mention that the position of the patient (typically head first, supine) should be indicated when preparing the PET acquisition. This ensures the correct orientation of the reconstructed images since in most cases, left/right cannot be reliably determined based on the images alone (in contrast to cranial/caudal and anterior/posterior orientations).

2.2 Injection of the tracer

When injecting the subject with the tracer, a cannula has to be in place (typically in an arm vein). Most often a bolus injection is given, sometimes in combination with a constant infusion of the tracer over the time period of the study to obtain a faster equilibrium (Carson (2000)).

In most human PET (or SPECT) imaging studies, only a very small amount of ligand is injected, often in the range of pico to nanograms. This usually requires a high specific activity, i.e. the amount of radioactively labelled versus unlabelled molecules, at the time of injection. E.g. if the specific activity of a ligand is $4 TBq/mmol$ at injection time and if we inject $400 MBq$, the total amount of ligand injected is $0.1 \mu mol$. When using certain tracers (e.g. $[^{11}C]$-Carfentanil, a highly potent and selective μ opioid receptor agonist) the total amount of compound administered has to be lower than some predefined value (e.g. $0.03 \mu g/kg$ body weight in case of $[^{11}C]$-Carfentanil), ensuring sub-pharmacological doses.

To know the exact amount of activity injected, the remaining dose after injection (rest dose) should be measured as well as the exact time of dose measurement, injection time and rest dose measurement. Accurate timing requires the same or cross-calibrated clocks. The effective dose injected can be calculated as:

$$D = D_i * e^{-\frac{ln(2)}{t_{1/2}}(t_0 - t_i)} - D_e * e^{-\frac{ln(2)}{t_{1/2}}(t_e - t_0)} \tag{1}$$

in which D is the effective dose injected at time t_0, D_i is the dose measured before injection at time t_i and D_e is the rest dose after injection as measured at time t_e. The half-life of the tracer is given by $t_{1/2}$.

2.3 PET measurement

Several high resolution PET scanners are available on the market for which the performance is well characterized. New clinical scanners typically operate as a PET-CT scanner in which the CT can be used for attenuation correction. For this purpose, a low dose CT, limiting the radiation exposure, is sufficient. However, there are still high resolution dedicated PET scanners in operation which most often use $^{68}Ga/^{68}Ge$ or ^{137}Cs sources for attenuation correction. The CT or PET scan used to correct for attenuation, sometimes called the transmission scan, is not performed simultaneously and therefore a mismatch between the head position during the transmission scan and the emission scan (i.e. the actual PET measurement) can occur. This will lead to artifacts and can give rise to large errors in the modelling. Therefore it is recommended that the coregistration between the transmission and the emission scans is explicitly evaluated by an expert. This can be done by reconstructing the PET emission image without attenuation correction and simultaneously viewing it with the reconstructed transmission scan.

PET measurements used for kinetic modelling are dynamic measurements. Two strategies are possible depending on the scanner: a list-mode acquisition or a dynamic acquisition in which time frames have to be specified before the start of the acquisition. List-mode acquisition has the major advantage that rebinning in frames can be done afterwards and - if necessary - another rebinning scheme can be used. However, due to the large amount of data (depending on the number of events and the length of the scan), the option of using multiple rebinning schemes is not always feasible in practice. The frame definition actually defines the sampling resolution of the dynamic PET study. Since we need to reconstruct every frame, two properties should be kept in mind: a frame should contain enough events to ensure a reliable reconstruction, and during a frame the distribution of the tracer should be more or less constant. These two requirements are not met in the beginning of the acquisition and a trade-off has to be chosen. Sampling is certainly not uniform with short frames in the beginning and gradually longer frames towards the end. An example of a frame definition used when performing a 60 minutes $[^{11}C]$-Flumazenil (a GABA-A antagonist) acquisition is 4 x 15s, 4 x 60s, 2 x 150s, 10 x 300s.

Since dynamic PET measurements are long, motion correction should be applied. First, by paying attention to patient comfort when positioning them in the scanner, by fixating the head, and by giving adequate instructions beforehand, major movements can be avoided. Second, coregistration of the different frames can be performed to correct for small movements (see later). Some groups are currently investigating how one can use tracking devices (e.g. Montgomery et al. (2006)) or, in case of the new MRI-PET scanners, simultaneous MRI scanning (Catana et al. (2011)) to continuously monitor any movement and to correct the list mode using these measurements. This is still work in progress but the initial results look promising.

Besides the frame definition, which only in case of list mode data can be changed after the acquisition, a number of settings are irreversible, i.e. they cannot be changed after the measurement. These are the time coincidence window, energy window, settings for scatter and random measurements, measurements for attenuation, start and duration of the scan, etc. Corrections for randoms, scatter and attenuation are necessary in brain imaging and are relatively easy to perform. Scatter correction has an impact on the final results but few studies have been done to quantify this. Attenuation correction is typically done when quantification is necessary but when using a PET transmission scan, this might add additional noise from the transmission scan through propagation into the reconstruction of the emission data. Nowadays, this is much less of a problem when using CT for attenuation correction since it is less noisy than a PET transmission scan.

Since often a bolus injection is given, dead time can be significant in the first minute. Adequate dead time correction is necessary in order to correctly measure the high initial activity. Therefore, the dead time correction available on the system should be well characterized.

The start and duration of the scan depend on the tracer and its kinetics as well as on the model that will be applied to determine the physiological parameters. In many applications it is common practice to start the scan at the time of injection although, for simplified methods, the scan can be started at later a time point when equilibrium is approached. The duration of the scan determines the amount of data generated. Furthermore, the duration is also determined by the system under study: we assume that the physiological and metabolic processes which

affect our measurement are more or less constant for the duration of the measurement, unless we explicitly want to manipulate these processes in e.g. activation studies.

Importantly, it is necessary to correct for decay of the isotope unless one takes this into account explicitly in the models. In this chapter we assume that decay correction has been performed.

2.4 Sampling of blood

A number of kinetic models that are commonly used in PET require the sampling of arterial blood to determine the arterial blood or plasma concentration which indicates how much tracer is available for uptake in the brain. This can be done by measuring radioactivity of the blood/plasma samples with a well counter and scaling this number by the volume measured. A major problem that arises with some tracers is that radioactive metabolites are formed which are also detected and indistinguishable from intact tracer, since we measure the isotope attached to a molecule and not the molecule itself. Often metabolites are formed outside the brain and do not cross the blood-brain-barrier. In such a case, the input function can easily be corrected by multiplying it with the intact fraction of the tracer at each time point. The intact fraction can be obtained by taking blood samples at different time points and analyzing them with high-performance liquid chromatography (HPLC) which separates intact tracer from metabolites based on different retention times (due to different chemical interactions) in a column .

For this procedure, it is required that the blood samples have a larger volume for accurate processing compared to the samples needed for the determination of the input function. Typically, 5-7 samples are taken and a model describing the intact fraction as function of time is fitted through the data points to obtain the intact fraction for every time within the measurement interval.

The most popular models used for this are:

1. The mono-exponential model given by

$$F(t) = Ae^{-\frac{ln(2)}{\alpha}t} \tag{2}$$

   describing the fraction $F(t)$ of intact tracer over time. The parameter A describes the amplitude, while α describes the biological half live. Sometimes an additional constraint $A = 1$ (i.e. at the time of the injection, we have 100% intact tracer) is imposed.

2. The bi-exponential model given by

$$F(t) = Ae^{-\frac{ln(2)}{\alpha}t} + Be^{-\frac{ln(2)}{\beta}t} \tag{3}$$

   in which A and B are the amplitudes of the two processes each described by a half-life α respectively β. An additional constraint $A + B = 1$ with the same interpretation as above can be imposed. An equivalent model is given by:

$$F(t) = Ae^{-\frac{ln(2)}{\alpha}(t-t_{delay})} + (1-A)e^{-\frac{ln(2)}{\beta}(t-t_{delay})} \tag{4}$$

   in which t_{delay} is a time-constant describing the delay before metabolisation takes place.

(a) Intact fraction of tracer

(b) Plasma input function
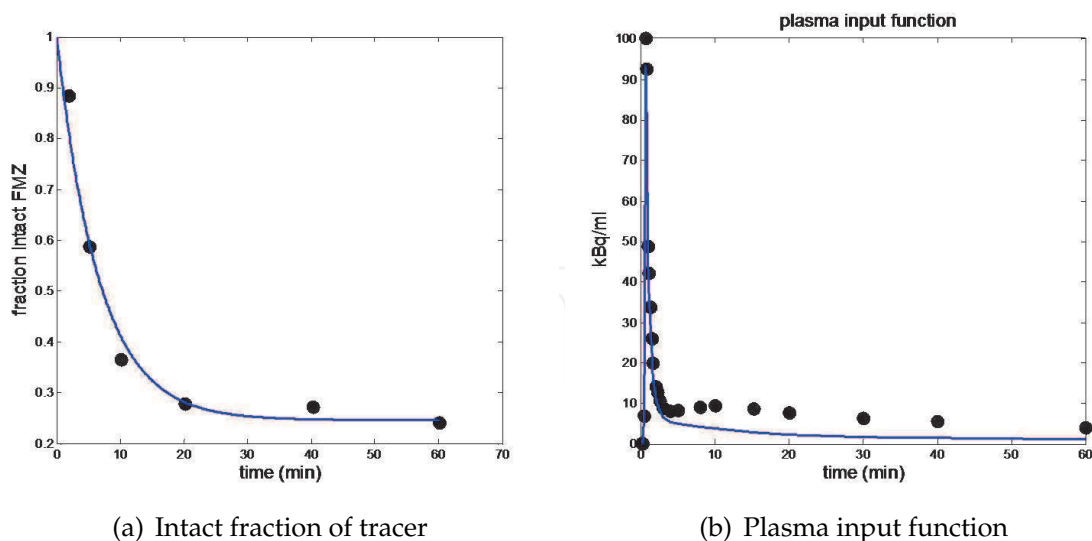
Fig. 1. Example of intact fraction and the plasma input function of $[^{11}C]$-Flumazenil

3. A third model is the Hill model described by:

$$F(t) = \frac{b}{1 + \left(\frac{a}{t}\right)^n} \tag{5}$$

in which a, b and n are parameters that can be interpreted respectively as the time to obtain half of the maximum value, the maximum value obtained at $t = 0$ if $n < 0$ (or the asymptotic value at infinity if $n > 0$) and the steepness of the slope. If $n < 0$ and $b = 1$, the Hill function starts at 1, then gradually decreases followed by a steep decrease and ending with a gradual decrease towards 0.

An example of calculating the intact fraction of $[^{11}C]$-Flumazenil is seen in figure 1 (left). The blue line indicates a fit of the bi-exponential model (equation 3) with the constraint $A + B = 1$ while the black dots represent the individual measurement points. The optimization was performed using multidimensional unconstrained nonlinear minimization (Nelder-Mead) implemented in Matlab. The initial value for the fitting parameters are $A = 0.5$, $\alpha = 10$ min and $\beta = 100$ min. The resulting fitted parameters are $A = 0.75$, $\alpha = 4.6$ min and $\beta = 4.32 * 10^{12}$ min. An example of a plasma input function is given in figure 1 (right). Black dots represent the measurement of each sample (corrected for decay) and the blue line is the input function after taking into account the intact fraction of tracer at each time point (using the fitted function obtained in figure 1 (left).

Unfortunately, this fitting procedure is not described in many publications but can have a major impact on the results. Furthermore, it is important to characterize the metabolites in terms of their effect on the PET measurement in the tissue of interest. If the contribution of the radioactive metabolite to the measured PET signal in the brain cannot be neglected, it should be incorporated into the kinetic model.

Several groups have looked at alternatives to determine the arterial input function. A popular approach is the so-called image-derived input function. Typically, a function which represents the input function is derived from the dynamic images by determining the time-activity curve in a small region including the carotid artery, positioned manually or (semi)automatically.

Due to the limited spatial resolution of the PET image this function has to be corrected for partial volume effects. Furthermore, activity in surrounding structures can affect this function through spill-in effects.

One way of correcting for these effects is to take into account a recovery coefficient (ratio of observed to true activity, estimated based on phantoms and computer simulations) and the spill-in fraction from surrounding tissue (obtained from a nearby ROI) (Chen et al. (1998)). Another option is to use a reconstruction algorithm with resolution recovery in combination with a high-resolution PET (Mourik et al. (2008)). A possible alternative strategy that does not use using any anatomical information, is to extract a time-activity curve by means of an independent component analysis (ICA), which implicitly accounts for spill-over effects (Naganawa et al. (2005)).

Depending on the method (e.g. the amplitude of the independent components is relative), the extracted image-derived input function may need to be scaled using the concentration determined in one or a few blood samples. Sometimes arterial samples can be replaced by venous samples (Chen et al. (1998)), usually at later time points when venous and arterial concentrations of tracer are almost equal. A more desirable alternative is to use so-called blood free methods. For example, Croteau et al. (2010) fitted a tri-exponential function to the extracted carotid time curve, using the carotid diameter as measured on MRI to correct for the partial volume effect. In Backes et al. (2009), the measured time-activity curve C_m was corrected as follows to obtain the image derived input function ($C_{input-ID}$):

$$C_{input-ID}(t) = \frac{C_m(t)}{a_v + (1 - a_v)(1 - e^{-kt})} \tag{6}$$

in which a_v is the fraction of vessel in the ROI and k is the rate constant for the transport to surrounding tissue. The main disadvantage of this method is that both parameters a_v and k have to be estimated empirically.

Recently, in Zanotti-Fregonara et al. (2011) different approaches to determine the image-derived input function were compared. The overall conclusion was threefold: 1) image-derived input functions have to be carefully evaluated for a particular tracer and setting, 2) blood samples are still necessary to obtain a reliable input function and 3) techniques which use the integral of the input function (e.g. the Logan plot) give better results compared to techniques in which the input function is used directly.

Another approach is to use a population based input function (usually in combination with one or a few venous blood samples) (Hunter et al. (1996), Hapdey et al. (2011)). A population based approach can also be used to correct an image derived input function for the intact fraction of tracer.

Importantly, blood/plasma samples are measured in a well counter, dose is determined by a dose calibrator and the activity in the brain is measured with PET. Each of these devices has a different sensitivity and performance (optimal range of activity which can be measured reliably). Since we need to combine the measurements in our modelling, the different machines need to be cross-calibrated.

A summary of the main points to consider for the acquisition is given in table 1.

Subject preparation	
	optimal positioning in scanner
	head fixation and comfort of the subject
Tracer injection	
	constant infusion or bolus injection
	effective dose injected
	amount of injected ligand / specific activity
Transmission scan	
	PET based (^{68}Ga/^{68}Ge or ^{137}Cs) or low-dose CT
Emission scan	
	list-mode or dynamic acquisition (frame definition)
	scanning parameters (start and end time, time coincidence window, ...)
	correction for decay, dead-time, scatter, randoms, ...
	cross-calibration with dose calibrator and well counter
	if possible: on-line motion correction
Other measurements	
	if input function needed
	image derived
	timing of blood samples
	arterial or venous samples
	if metabolite correction needed
	timing of arterial samples
	model to describe intact tracer fraction
	EEG, ECG, blood pressure, ...

Table 1. Main points to consider for the acquisition.

3. Reconstruction

Each frame is reconstructed into a 3D image. There are two major classes of reconstruction: filtered back projection and iterative reconstruction. Filtered back projection has the advantage that it is fast and robust but the disadvantage that in low count measurements streak artifacts occur in the reconstructed images. Iterative reconstruction techniques have the advantage that a-priori information can be taken into account (e.g. the noise model, scatter and attenuation measurements) avoiding precorrection of the raw data before reconstruction which results in superior image quality. The disadvantage is that convergence is not uniform throughout the image making it sensitive to bias due to the limited number of iterations that is often applied. Reconstruction time is also much longer compared to filtered back projection. A very popular and widely used method is OSEM (ordered subsets expectation maximization). This method includes a Poisson-noise model and has a non-negativity constraint. The latter can cause some bias in the parameters estimated when modelling the data. Several studies (Boellaard et al. (2001), Oda et al. (2001), Belanger et al. (2004), Morimoto et al. (2006)) have compared iterative reconstruction methods with filtered back projection. The overall conclusion was that both methods have a similar quantitative accuracy although in some situations, filtered back projection may still be preferable. In a more recent study by Reilhac et al. (2008), using simulations, it was shown that the positivity constraint in maximum likelihood expectation maximization (MLEM)-based algorithms leads to overestimation of the activity in regions with low activity (e.g. in a reference region) which causes a significant bias

in binding potential estimates. However, the use of a resolution model reduces low-statistics bias (Walker et al. (2011)).

Usually, the dynamic PET data are reconstructed frame by frame in an independent way without taking into account the temporal relationship between subsequent frames. To overcome this shortcoming, a 4D reconstruction has been developed in which all frames are reconstructed simultaneously (for a recent overview, see Rahmim et al. (2009)). During this 4D reconstruction, different techniques (e.g. iterative temporal smoothing, wavelet based techniques to control noise) can be used to handle temporal information. A particularly interesting approach is to model the data directly from the sinograms. This was first described by Maguire et al. (1996) and is now more widely studied in the context of 4D reconstruction. Because it is rather difficult to model the noise distribution in reconstructed images, the spatially variant noise distribution is neglected when doing kinetic modelling. By calculating sinograms of the physiological parameters directly from the raw data this problem can be circumvented. These sinograms are subsequently reconstructed to form parametric images. The best results with this approach so far have been obtained when using a Gjedde-Patlak model as shown by Wang et al. (2008), and Wang and Qi (2009), but other models are also possible.

Another new development is the use of anatomical knowledge that is available from other imaging modalities (like MRI). One such a technique is the anatomically based maximum a posteriori reconstruction (A-MAP) (Baete et al. (2005)), which corrects the images for partial volume effects, the importance of which is described in the next section.

A summary of the main points to consider for the reconstruction is given in table 2.

Definition of frames (rebinning from list mode)
Pre-corrections if necessary (e.g. random correction)
Reconstruction method: iterative reconstruction or filtered back-projection
reconstruction time
inclusion of additional measurements (scatter, attenuation, . . .)
filtering
effect of reconstruction on final results (bias, variance, resolution)
Optionally, take into account:
temporal relation between frames (4D reconstructions)
anatomical knowledge (partial volume correction)
Data management
Quality assurance of reconstructed images

Table 2. Main points to consider for the reconstruction

4. Processing

Since dynamic PET measurements are long, patient movement is almost inevitable and motion correction should be applied. Implicit in the previous step of reconstruction is that either the transmission scan or the CT scan are in (near) perfect spatial alignment with the PET frames to be attenuation corrected. Also, the different PET frames themselves should be spatially aligned since the next step of kinetic modelling assumes that the time course (in voxels or areas) is derived from the same location.

Motion correction poses two particular difficulties: the first frames are too noisy to use and any movement occurring during a frame is neglected. The first issue can be solved by creating a sum image of the first few minutes reasonably assuming that there was no significant motion during this period and by coregistering all subsequent frames to this sum image. The second issue is more problematic, but as long as movements are small (i.e. less than a few mm in displacement or a few degrees in rotation) this leads to limited additional blurring of the image and will not cause a major problem.

Realigning PET frames to the first frame or a sum image can be done by simply minimising the intensity differences between the images, but in some cases it may be necessary to use more complex measures of similarity between the images based on more general information than simple intensity, such as mutual information or cross correlation. Examples of such situations are when tracer uptake patterns differ drastically over time or when one needs to coregister another imaging modality (e.g. a CT or MRI image) to a PET frame. When realigning within an imaging modality (e.g. PET frames) rigid (6 parameters: 3 translational and 3 rotational parameters) spatial transformations are usually sufficient. Coregistrations between different modalities benefit from affine (12 parameter) transformations allowing additionally 3 directions of zoom and of skew although a rigid body transformation is often acceptable.

Having a high resolution structural scan, usually a T1-weighted MRI, of the same subject coregistered to the PET scan may serve multiple purposes. First, the MRI can be used to draw anatomical volumes of interest (VOIs) for subsequent kinetic modelling with much higher precision than is possible based on PET scans and, importantly, unbiased from the pattern of tracer uptake. Second, the structural scan can be used to calculate a potentially more precise (due to higher resolution of the source image) spatial transformation that takes the subject's brain into a common stereotactic space, such as Montreal Neurological Institute (MNI) space. This allows direct comparisons across subjects in this standard space. Alternatively, the obtained spatial transformation can be inverted and applied to MNI space VOI templates to bring them into the subject's native space if one prefers to avoid interpolation issues and working on distorted images. Third, the structural scan provides high resolution anatomical information needed to perform partial volume correction.

The partial volume effect (PVE) stems from the relatively low spatial resolution of the PET scanner. This can be quantified by means of the system's point spread function (PSF), which describes the degree to which a point source is 'blurred' by the imaging system. More specifically, when imaging a radioactive point source (perfect impulse function), this object appears larger but less intense (bell shaped curve), since the total number of counts is preserved. Applied to brain imaging, this means that for structures that are smaller than the sampling resolution (about 4 mm FWHM for modern scanners), e.g. the cortex, the measured signal is a mix of the true radiotracer concentrations in the multiple tissue types present. As such, the measured activity in grey matter is affected by spill-out onto other tissues (e.g. CSF) and spill-in from adjacent white matter.

This effect poses a particular problem when one wishes to study decreases in tracer binding in patients. A lower measured signal could mean a true decrease in tracer binding, PVE due to tissue atrophy or a mixture of both. In order to disentangle these effects, a formal partial volume correction (PVC) can be applied, based on prior higher resolution knowledge about the underlying tissue types and the point spread function of the scanner.

The basic idea is to view the measured PET signal as a convolution of the true image by the PSF and correct the measured PET signal in a voxel/region by modelling it as a combination of effects in the various tissue types present, taking into account the proportion of those tissue classes in that voxel/region.

The prior anatomical knowledge is derived from a high resolution structural scan, nowadays usually an MRI scan, which is segmented into the tissue types of interest, commonly taken to be grey matter, white matter and cerebrospinal fluid (CSF). The image values in such segmentation maps (e.g. a voxel with a value of 0.8 in a grey matter map) can be interpreted as the tissue fraction (80% of the voxel consists of grey matter) or probability (80% chance that the voxel belongs to grey matter). Importantly, the quality and accuracy of these segmentations will propagate into the partial volume corrected PET images. .

Here, for illustrative purposes, we describe a commonly used method, the Müller-Gärtner partial volume correction (Müller-Gärtner et al. (1992)), to correct the activity in grey matter tissue.

$$I_{GM} = \frac{I_{measured} - (I_{WM}P_{WM}) \otimes PSF - (I_{CSF}P_{CSF}) \otimes PSF}{P_{GM} \otimes PSF} \qquad (7)$$

where I_{GM} is the partial volume corrected image, $I_{measured}$ the original PET image, I_{WM} and I_{CSF} the tracer uptake in white matter and CSF, P_{GM}, P_{WM} and P_{CSF} the tissue probabilities, and PSF the system's point spread function.

The corrected image value I_{GM} is obtained by subtracting from the measured value $I_{measured}$ the contributions of white matter and CSF signal. These contributions are given by the tissue's tracer uptake e.g. I_{WM} weighted by the proportion P_{WM} of that particular tissue class in the voxel/area and convolved with the PET system's PSF to match the resolution of the higher-resolution tissue probability maps with the PET image. In order to obtain 'pure' grey matter tracer uptake (i.e. independent of how much grey matter is present in the voxel/area), the result is divided by the proportion of grey matter P_{GM}, again convolved with the PSF.

The PSF of a PET system can be measured and varies spatially, being the most narrow at the centre of the scanner. For brain scans, this spatial variability is thought to be negligible. P_{GM}, P_{WM} and P_{CSF} are derived from the tissue probability maps. Under the assumption that tracer uptake is homogeneous throughout white matter, a representative uptake value for I_{WM} can be obtained by measuring the PET signal within a 'pure' WM area where there is no significant spill-in from other tissues, such as the centrum semiovale. Likewise I_{CSF} can be derived from a pure CSF region or can be assumed to be zero since CSF should not show any tracer uptake.

While the Müller-Gärtner PVC is a postprocessing method performed after image reconstruction, a similar strategy can be applied during iterative reconstruction incorporating anatomical information as a priori knowledge, such as A-MAP (Baete et al. (2005)). The latter approach offers a better spatial resolution, since smoothing (which is done during reconstruction in order to suppress noise) can be restricted to a specific tissue class instead of increasing spill-over between tissue classes, yielding sharper anatomical boundaries.

PVC can be applied on a voxel- or VOI-based level, the advantages and disadvantages of which are discussed in more depth later. Errors in registration of tissue maps to the PET image, misclassifications in the tissue probability maps, and VOI misplacement may all introduce errors that propagate in further analyses on partial volume corrected data.

Theoretically, PVC would preferably be applied prior to kinetic modelling, since there is usually not a simple linear relationship between raw counts and kinetic modelling output measures that are eventually used to describe processes of interest.

Images can be smoothed prior to kinetic modelling (parametric imaging), or are smoothed implicitly by using the VOI approach. Either method will attempt to find the kinetic modelling coefficient that best describe the data, either in each voxel or in each VOI independently of the other voxels/VOIs.

A summary of the main points to consider for the processing is given in table 3.

Motion correction
> sum the first frames (e.g. first 5 minutes assuming no movement)
> align all images of the remaining frames
>> method
>> evaluation of motion parameters

Coregistration with high-resolution anatomical MRI
> method (transformation, cost-function)
> PET image (e.g. summed image of all frames)

Use high-resolution anatomical MRI
> to draw volumes of interest
> to correct for partial volume effects
> to determine the spatial transformation to a common anatomical space

Smoothing of PET data (noise reduction)

Table 3. Main points to consider for image processing

5. Kinetic models

5.1 Pharmacological terminology

When describing the pharmacokinetics of a tracer, the most commonly used method is a compartmental model (figure 2), where distinct pools of tracer (spatial location or chemical state) are assigned to different compartments. It is assumed that the tracer concentration in a compartment, given by C (e.g. expressed in Bq ml^{-1}), is homogeneous (instantaneous mixing assumption). The rate of exchange of tracer between 2 compartments is given by a rate constant k (in fraction per time, e.g. min^{-1}).

The rate at which the tracer crosses the blood-brain barrier (BBB) to enter the first brain compartment is given by K_1, the only rate constant historically denoted in upper case and having units of ml plasma per cubic cm tissue per min (ml cm^{-3} min^{-1}). This rate constant for blood-brain barrier transport is related to perfusion (blood flow).

In a capillary model, the following relation can be derived

$$K_1 = EF \tag{8}$$

where E is the unidirectional extraction from blood into brain during the tracer's first pass through the capillary bed, and F denotes the blood flow. Regarding the capillary as a rigid tube, the Renkin-Crone model posits that

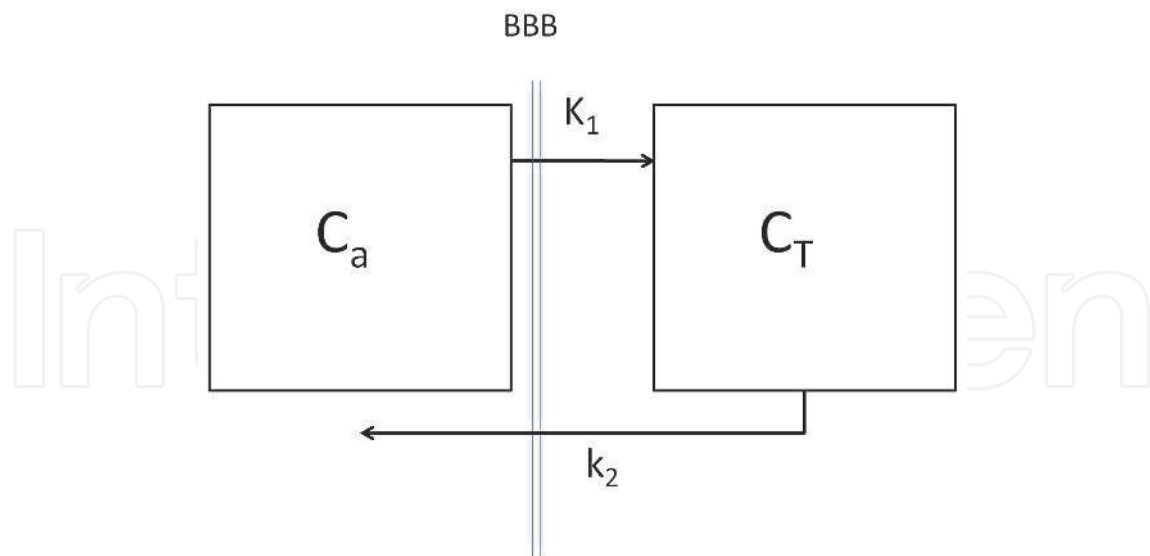$$E = 1 - e^{-\frac{PS}{F}} \tag{9}$$

BBB

Fig. 2. One-tissue compartement model

with PS the permeability surface product (the tracer's total permeability across the capillary membrane).

On one end of the spectrum, for tracers with a large permeability surface product (freely diffusible tracers e.g. water), extraction is virtually independent of perfusion and approaches 1 (the exponential term is very small). As a result, K_1 approximates blood flow for such tracers. On the other end, for tracers with a permeability surface product much lower than the blood flow, E can be approximated by PS/F and hence K_1 is no longer related to blood flow but is proportional tot the permeability surface product ($K_1 \approx PS$).

Two interacting compartments commonly found in a model are ligand and receptor. A ligand is a chemical that binds to a receptor. If this binding results in a chemical response i.e. 'activates' the receptor, the ligand is called an agonist. More specifically, the term 'agonist' is used for molecules that induce a pharmacological response mimicking the action of the naturally occurring compound, e.g. the binding of morphine to opioid receptors mimics the action of the endogenous endorphins. An 'inverse agonist' induces the opposite pharmacological response as the agonist. Finally, a ligand is called an antagonist if its binding does not activate the receptor or appears to 'deactivate' it by displacing an agonist.

Receptor occupancy refers to the percentage of receptors that are currently being occupied by ligands. The aim of PET receptor displacement studies is to detect changes in receptor occupancy caused by the experimental action of introducing a nonradioactive ligand. By measuring the difference in binding of the radioactive tracer, which is applied before and after the pharmacological challenge, the occupancy of the nonradioactive ligand can be inferred. For example, if the non-radioactive compound occupies 25% of binding sites, relative tracer binding will decrease by around 25% as well. This is explained in more detail in a later section.

In vitro, ligand-receptor kinetics is described by the well-known Michaelis-Menten relationship for a reversible binding.

$$L + R \; \underset{k_{\text{off}}}{\overset{k_{\text{on}}}{\rightleftharpoons}} \; LR$$

(10)

where L = ligand, R = receptor, LR = ligand-receptor complex, k_{on} = rate constant of association and k_{off} = rate constant of dissociation. According to the law of mass action, the kinetics of this system are described by

$$\frac{dC_{LR}}{dt}(t) = k_{on}C_L(t)C_R(t) - k_{off}C_{LR}(t)$$

(11)

with C_L, C_R and C_{LR} being the concentration of respectively L, R and LR.

When the system reaches a dynamic equilibrium:

$$k_{on}C_LC_R = k_{off}C_{LR}$$

(12)

Rearranging the previous equation gives the definition of the dissociation constant, K_D:

$$K_D = \frac{k_{off}}{k_{on}} = \frac{C_LC_R}{C_{LR}}$$

(13)

The affinity of a receptor for the ligand is defined as $1/K_D$.

Furthermore, the total concentration of receptors, free and bound, or receptor density is

$$B_{max} = C_{LR} + C_R$$

(14)

Here we have assumed that none of the receptors are bound by endogenous ligands.

Rearranging the two previous equations gives

$$C_{LR} = \frac{B_{max}C_L}{K_D + C_L}$$

(15)

This relationship is termed a saturation binding curve. B_{max} is the asymptotic value representing the occupation of all available receptors. K_D is the concentration of ligand at which 50% of all receptors have been saturated (if $C_L = K_D$, then $C_{LR} = 0.5B_{max}$). The initial slope of the saturation curve is B_{max}/K_D.

The *in vitro* binding potential is defined as

$$BP = \lim_{C_L \to 0} \frac{C_{LR}}{C_L}$$

(16)

Since PET studies employ tracer doses (i.e. occupying a negligible percentage of receptors, often taken to be 5%), the concentration of free ligand is very small compared to K_D and hence may be ignored. Using equation 15, BP can be written as:

$$BP = \frac{B_{max}}{K_d}$$

(17)

It is usually assumed that changes in BP are mainly due to changes in total number of receptors (B_{max}) while affinity (=$1/K_D$) of the tracer for the receptor is similar. While *in vitro* ligand binding consists of a single compartment, *in vivo* PET models include plasma and one or more tissue compartments, thus requiring a slightly different definition of BP, as will described in more detail later.

A related concept to BP is the volume of distribution (or distribution volume). Similar to BP, there are also slightly different *in vivo* definitions of the volume of distribution, which will be discussed later. In its original pharmacological definition, the apparent volume of distribution is the virtual plasma volume that the drug would have to occupy in order to adopt the same (uniformly distributed) concentration in the body as in the blood plasma. Put differently, it is the ratio of the total drug amount in the body (administered dose) over the drug's plasma concentration (at equilibrium). For example, if 5 mg of a drug is present in the body, and its plasma concentration is 250 ng per ml, then a virtual volume of 20 l plasma would be needed to contain 5 mg of the drug.

In PET, the volume of distribution V_T is based on a similar conceptual idea but has been adapted slightly: it relates to a specific organ of interest instead of the entire body and uses the tracer's concentration (amount per volume) instead of volume (Innis et al. (2007)).

$$V_T = \frac{C_T}{C_a} \tag{18}$$

where C_T is the tracer's concentration in the tissue and C_a is the tracer's arterial plasma concentration, assuming equilibrium has been reached. Hence, its values are expressed in ml per cm^3 which is in fact unitless since 1 ml = 1 cm^3. For example, if the tracer's concentration is 50 kBq cm^{-3} in the brain and 2.5 kBq ml^{-1} in plasma, then V_T is 20, or, in other words: in order to have the same amount of tracer as in 1 cm^3 of brain, 20 ml of plasma would be needed.

In contrast to the *in vitro* definition of binding potential, the *in vivo* situation is much more complex. A fraction f_p of tracer is bound to plasma proteins and will not pass the blood brain barrier. Usually, a reliable estimate of this fraction is difficult. Another fraction of intact tracer is protein bound in the brain (non-specific binding representing the non-displaceable compartment). The free fraction of tracer available for binding to the receptor is denoted f_{ND} according to the consensus nomenclature (Innis et al. (2007)). Therefore, three different definitions of binding potential in PET exist which can be expressed as a ratio at equilibrium:

1. BP_F: the ratio of the concentration of specifically bound tracer to the concentration of free tracer in tissue. We assume that the concentration of free tracer in tissue equals the concentration of free tracer in plasma.

2. BP_P: the ratio of the concentration of specifically bound tracer in tissue to the concentration of intact tracer in plasma (both free and protein bound).

3. BP_{ND}: the ratio of the concentration of specifically bound tracer in tissue to the concentration of non-displaceable tracer in tissue.

There is a linear relation between these three values: $BP_{ND} = f_{ND}B_F$ and $BP_P = f_pB_F$.

Analogous to the different definitions of binding potential, different definitions exist for the volume of distribution. The total tracer concentration C_T in tissue can be written as the sum of three different parts:

$$C_T = C_{LR} + C_{NS} + C_L \tag{19}$$

in which C_{LR} is the concentration of tracer bound to the receptor, C_{NS} is the concentration of nonspecific bound tracer and C_L is the concentration of free available tracer. The concentration of the non-displaceable part is given by $C_{ND} = C_L + C_{NS}$. Besides V_T, the volume of distribution of all radioligand, we also define the distribution volume of the non-displaceable part of the tracer as:

$$V_{ND} = C_{ND}/C_a. \tag{20}$$

Note that in an *in vivo* setting, B_{max} should actually be replaced by B' which is the maximum concentration of available receptors, i.e. not occupied by endogenous ligands or compartmentized in a low affinity state.

The binding potential that we measure with PET is BP_{ND} and the relation with the volume of distribution is:

$$BP_{ND} = \frac{V_T - V_{ND}}{V_{ND}} = \frac{V_T}{V_{ND}} - 1 = DVR - 1 \tag{21}$$

with DVR the volume of distribution ratio.

BP and V_T are combinations of the rate constants introduced in the compartmental models as will be shown in a later section.

A common assumption in compartmental modelling is that the underlying physiological processes are not influenced by the presence of the tracer and are in a steady-state, i.e. the rate constants do not change over time. In this case, linear differential equations can be used to describe how changes in concentration in one compartment influence concentration in another one. The tissue compartments can refer to physical locations (e.g. outside vs. inside the cell) or chemical states (e.g. free vs. bound ligand).

The general aim is to estimate one or more of the rate constants, either individually or in some combination such as BP and V_T. The parameter estimation is based on the measured PET signal in the brain and the concentration in arterial blood measured by the arterial input function.

5.2 Model simplification

Accurate models describing the full behaviour of a tracer are too complex to be used in practice. Therefore, model simplifications are used. We show here the example of the well-known tracer $[^{18}F]$-FDG used when measuring the metabolic rate of glucose consumption. In figure 3, a model for the PET tracer $[^{18}F]$-FDG, consisting of both physical spaces (vascular, interstitial and cellular) and chemical compartments (FDG and FDG-6-PO$_4$) is shown. Constants K_1, k_2, k_5 and k_6 describe the rate of transport of FDG between the physical compartments, while rate constants k_3 and k_4 give the phosphorylation and dephosphorylation rates respectively. The blood-brain-barrier is indicated by BBB.

The transport of glucose or FDG across the cell membrane in cerebral tissue is very fast as compared with the transport across the capillary wall and the phosphorylation reaction catalyzed by hexokinase. The concentration ratio between the interstitial space and the cellular space is nearly in equilibrium at all times. Therefore, the interstitial and the cellular space can be approximated as a single compartment. This leads to the well-known two-tissue compartment of $[^{18}F]$-FDG (figure 4). In addition in the brain almost no dephosphorylation of FDG-6-PO$_4$ takes place within the first hour which leads to a further simplification in which $k_4 = 0$.
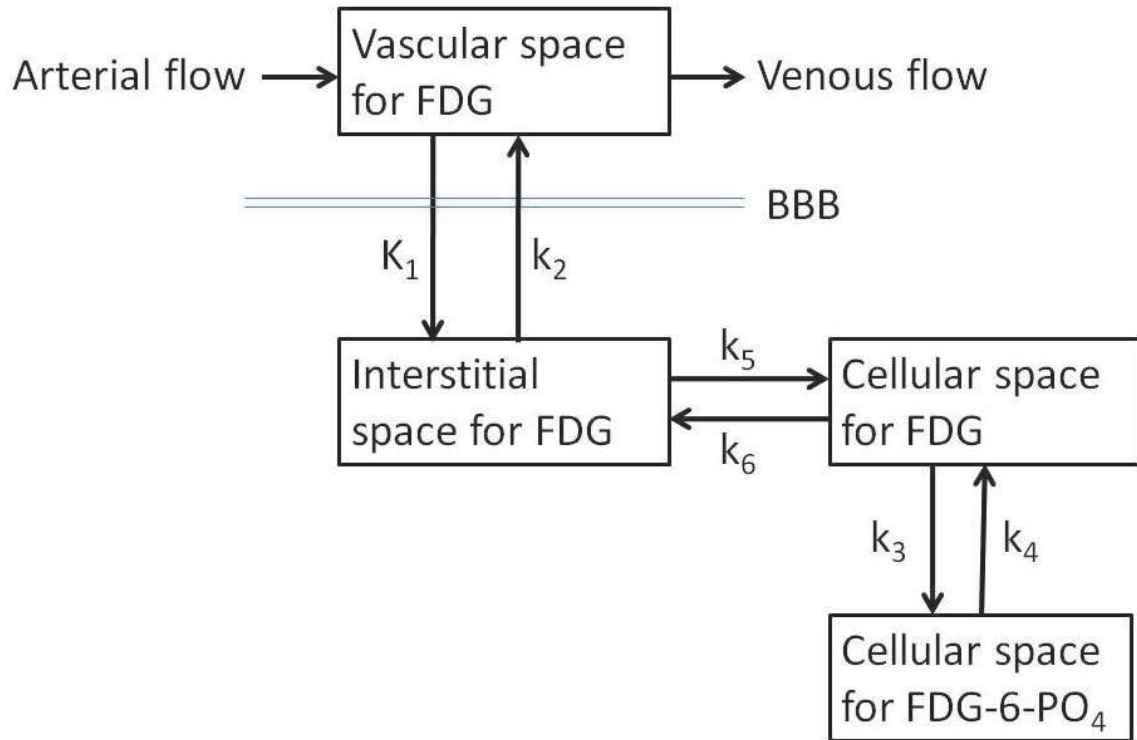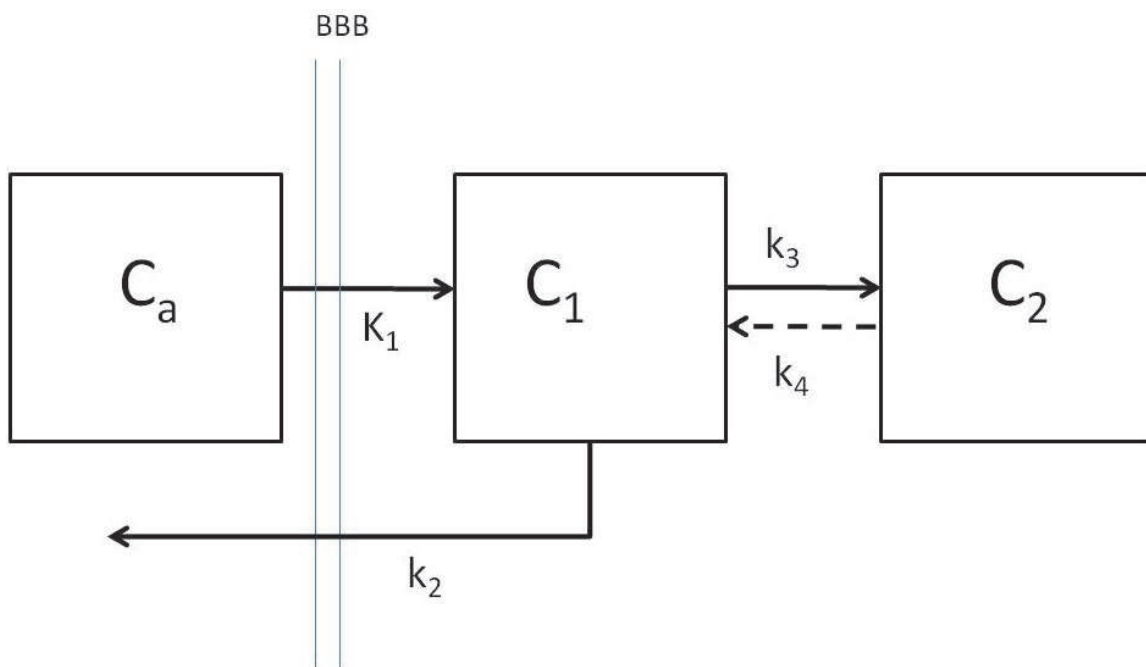
Fig. 3. Extended FDG model

Fig. 4. simplified FDG model

FDG and glucose behave differently because FDG becomes trapped after phosphorylation. Influx/uptake of FDG is only proportional to the influx/uptake of glucose. The constant of proportionality is called the lumped constant LC.

5.3 Compartmental models

5.3.1 One-tissue compartment model

In the one-tissue compartment model, we have two rate constants K_1 and k_2 describing the model (see figure 2). The differential equation is given by:

$$\frac{dC_T}{dt}(t) = K_1 C_a(t) - k_2 C_T(t), \tag{22}$$

where C_a is the arterial plasma concentration of intact tracer and C_T is the concentration of tracer in tissue. This model is also called the Kety-Schmidt model originally developed to model tracers measuring regional cerebral blood flow.

The solution of this equation is given by:

$$C_T(t) = K_1 \int_0^t e^{-k_2(t-s)} C_a(s) ds = K_1 e^{-k_2 t} \otimes C_a \tag{23}$$

Using this expression, the rate constants can be estimated based upon the measurement of C_a and C_T at different time points. This estimation is a nonlinear operation.

A linear alternative can be formulated by integrating both sides of the differential equation 22:

$$C_T(t) - C_T(0) = K_1 \int_0^t C_a(s) ds - k_2 \int_0^t C_T(s) ds. \tag{24}$$

Assuming $C_T(0) = 0$, we find the following linear relation:

$$\frac{C_T(t)}{\int_0^t C_a(s) ds} = K_1 - k_2 \frac{\int_0^t C_T(s) ds}{\int_0^t C_a(s) ds}. \tag{25}$$

From this equation, K_1 and k_2 can be estimated using linear regression. The distribution volume can then be calculated as:

$$V_T = \frac{K_1}{k_2}. \tag{26}$$

5.3.2 Two-tissue reversible compartment model

In the two-tissue compartment model, K_1 and k_2 again describe the exchange of tracer with the blood pool similar as in the one-tissue compartment model. Two additional rate constants, k_3 and k_4, model the interactions between the 2 tissue compartments.

Tracer behaviour in this model (5) is described by the following set of differential equations:

$$C_T(t) = \frac{dC_{f+ns}}{dt}(t) = K_1 C_a(t) - (k_2 + k_3) C_{f+ns}(t) + k_4 C_b(t)$$

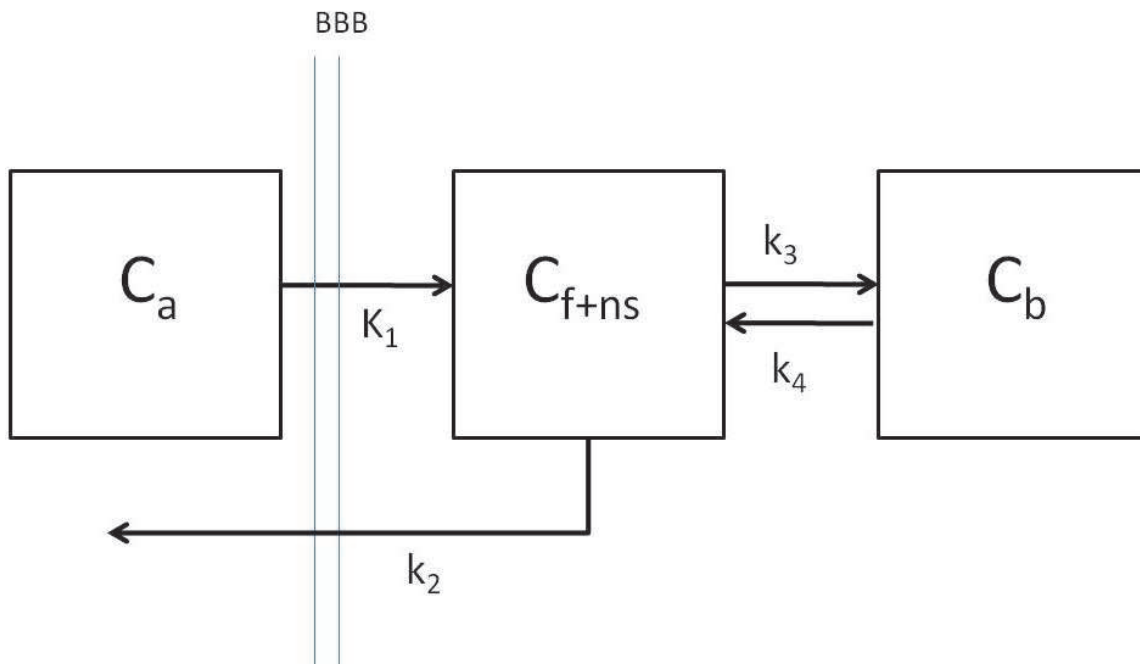$$\frac{dC_b}{dt}(t) = k_3 C_{f+ns}(t) - k_4 C_b(t)$$

Fig. 5. Two-tissue reversible compartment model

where C_{f+ns} denotes the concentration of free and non-specifically bound tracer and C_b is the concentration of specifically bound tracer. Reworking these equations gives

$$C_{f+ns}(t) + C_b(t) = (\phi_1 e^{-\theta_1 t} + \phi_2 e^{-\theta_2 t}) \otimes C_a(t) \qquad (27)$$

$$\phi_1 = \frac{K_1(\theta_1 - k_3 - k_4)}{\Delta}$$

$$\phi_2 = \frac{K_1(\theta_2 - k_3 - k_4)}{-\Delta}$$

$$\theta_1 = \frac{k_2 + k_3 + k_4 + \Delta}{2} \qquad (28)$$

$$\theta_2 = \frac{k_2 + k_3 + k_4 - \Delta}{2} \qquad (29)$$

$$\Delta = \sqrt{(k_2 + k_3 + k_4)^2 - 4k_2 k_4} \qquad (30)$$

The distribution volume is given by:

$$V_T = \frac{K_1}{k_2}\left(1 + \frac{k_3}{k_4}\right) \qquad (31)$$

An example of a time-activity curve in a right frontal region in a normal subject injected with [11C]-FMZ and the corresponding fit obtained using the two-tissue compartment model, is given in figure 6. The initial values for the rate constants were: $K_1 = 0.300$ ml cm^{-3} min^{-1}; $k_2 = 0.100$ min^{-1}; $k_3 = 0.050$ min^{-1}; $k_4 = 0.030$ min^{-1} and the fitted values were $K_1 = 0.302$ ml cm^{-3} min^{-1}; $k_2 = 0.076$ min^{-1}; $k_3 = 0.010$ min^{-1} ; $k_4 = 0.041$ min^{-1}. We also fitted the fraction of blood in the VOI (see below): the initial value was $V_b = 0.05$ and the fitted value was $V_b = 0.08$.
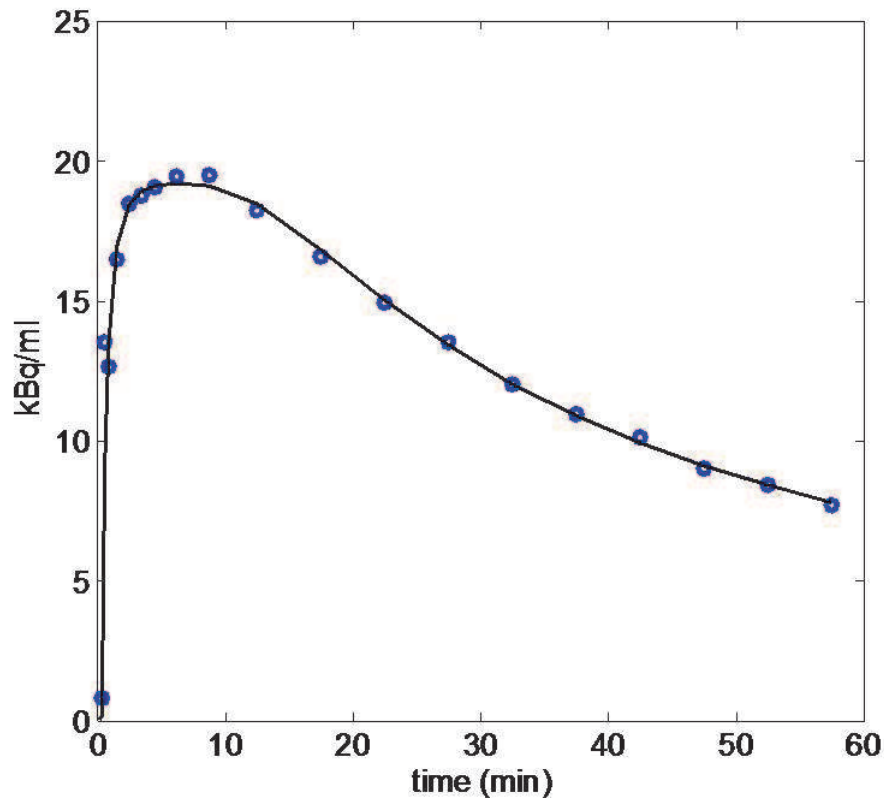
Fig. 6. Measured time activity curve (dots) and the corresponding fit (full line) using a two-tissue compartment model

5.3.3 Two-tissue irreversible compartment model

In case of irreversible binding, e.g. FDG, k_4 can be assumed to be 0 and the compartmental model equations simplify to:

$$\frac{dC_{f+ns}}{dt}(t) = K_1 C_a(t) - (k_2 + k_3)C_{f+ns}(t)$$

$$\frac{dC_b}{dt}(t) = k_3 C_f(t)$$

$$C_T(t) = C_{f+ns}(t) + C_b(t) = \{\frac{K_1 k_2}{k_2 + k_3}e^{-(k_2+k_3)t} + \frac{K_1 k_3}{k_2 + k_3}\} \otimes C_a(t) \tag{32}$$

$$K_I = \frac{K_1 k_3}{k2 + k3} \tag{33}$$

K_I is the net influx constant, the overall net rate of tracer uptake into tissue.

5.4 Graphical models

5.4.1 Gjedde-Patlak approach

This is an example of a graphical method which is derived using the assumption that $k_4 = 0$ (irreversible tracer) and that there is a steady state between the tissue concentration in the

reversible compartment and the blood or plasma concentration. Under these conditions we find:

$$\frac{C_T(t)}{C_a(t)} = K_I \frac{\int_0^t C_a(s)ds}{C_a(t)} - \frac{K_1 k_2}{(k_2 + k_3)^2} \qquad (34)$$

with C_T being the tissue concentration, C_a the arterial blood or plasma concentration, K_I is given by equation (33) and K_1, k_2 and k_3 the time independent rate-constants. Equation (34) is an asymptotic relation but in practice the steady state is reached within 20-30 minutes for tracers like $[^{18}F]$-FDG. The time after which we *assume* steady state is denoted by t^*.

5.4.2 Logan approach

For tracers with reversible binding kinetics, the following linear regression can be performed, assuming the relationship becomes linear (steady-state) after $t = t^*$:

$$\frac{\int_0^t C_T(s)ds}{C_T(t)} = A + V_T \frac{\int_0^t C_a(s)ds}{C_T(t)} \qquad (35)$$

The slope V_T is the distribution volume given by equation (31) and the intercept is given by $A = -\frac{k_2 k_4}{k_2 + k_3 + k_4}$.

Figure 7 shows an example of a time-activity curve of $[^{11}C]$flumazenil (FMZ) transformed according to the above formula in which $X = \frac{\int_0^t C_a(s)ds}{C_T(t)}$ and $Y = \frac{\int_0^t C_T(s)ds}{C_T(t)}$. The estimated value for $V_T = 4.89$ and t^* was chosen as $t^* = 20min$.

5.5 Reference models

5.5.1 Reference Tissue Model (RTM)

Sometimes, the arterial input function can be replaced by a reference region providing an indirect input function. More specifically, in this reference region there should be no specific tracer binding, hence making it possible to estimate the contribution of non-specific tracer binding to the signal in the tissue of interest (Lammertsma et al. (1996)).

Figure 8 depicts a reference tissue model, described by the following differential equations:

$$\frac{dC_r}{dt}(t) = K_1' C_a(t) - k_2' C_r(t)$$

$$\frac{dC_{f+ns}}{dt}(t) = K_1 C_a(t) - (k_2 + k_3)C_{f+ns}(t) + k_4 C_b(t)$$

$$\frac{dC_b}{dt}(t) = k_3 C_{f+ns}(t) - k_4 C_b(t)$$

where C_r is the nonspecific tracer concentration (and the measured PET signal) in the reference region, and K_1' and k_2' are the rate constant describing resp. tracer influx into and outflow from the reference tissue. The two lower equations are those of the standard 2-tissue compartment model described higher, with $C_T(t) = C_{f+ns}(t) + C_b(t)$.

It is assumed that the volume of distribution of the non-specifically bound tracer is similar in both the tissue of interest and the reference region, i.e. $K_1/k_2 = K_1'/k_2'$. Hence, C_T can be
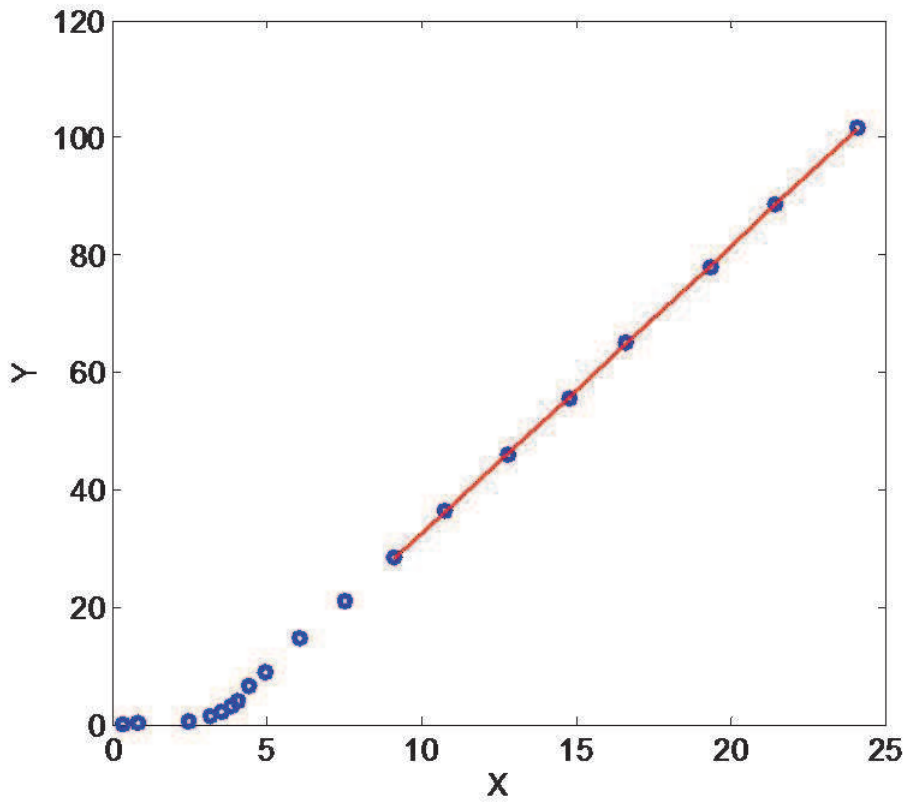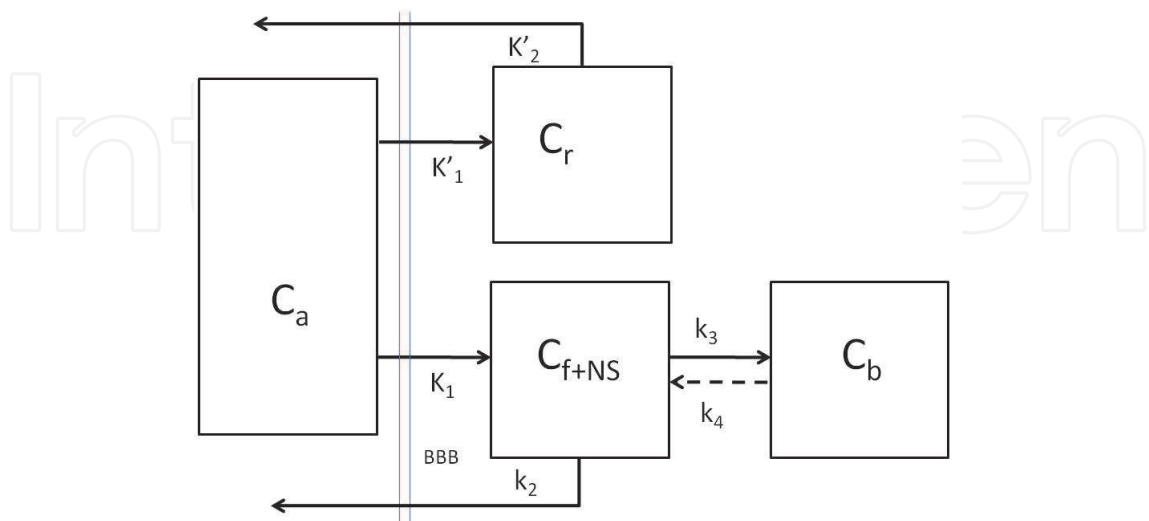
Fig. 7. Logan plot

Fig. 8. Reference tissue model

described as a function of C_r omitting the need for the arterial input function C_a. The solution is given by:

$$C_T(t) = R_1[C_r(t) + A_1 e^{-\theta_1 t} + A_2 E^{-\theta_2 t}] \otimes C_r \tag{36}$$

with

$$A_1 = \frac{\theta_1 - k_3 - k_4}{\Delta}(\frac{k_2}{R_1} - \theta_1)$$

$$A_2 = \frac{k_3 + k_4 - \theta_2}{\Delta}(\frac{k_2}{R_1} - \theta_2)$$

$$R_1 = \frac{K1}{K_1'} \tag{37}$$

and the parameters θ_1, θ_2 and Δ are given by equations (28-30). The parameters R_1, k_2, k_3 and k_4 have to be estimated.

5.5.2 Simplified Reference Tissue Model (SRTM)

The reference tissue model can be further simplified if it can be assumed that the free and bound compartments of the tissue of interest are not readily distinguishable, i.e. can be described by one compartment. This reduces the number of parameters to be estimated from four to three, reducing standard errors on the estimates and speeding up convergence. The solution in this case is given by (Lammertsma & Hume (1996)):

$$C_T(t) = R_1 C_r(t) + k_2(1 - \frac{R_1}{1 + BP_{ND}})C_r \otimes e^{-\frac{k_2 t}{1 + BP_{ND}}} \tag{38}$$

with R_1 given by equation (37). The parameters R_1, k_2, and B_{ND} have to be estimated.

5.5.3 Reference logan

The Logan approach described above can also be applied when using a reference region instead of the arterial input function. In that case the operational equation becomes (Logan et al. (1996)):

$$\frac{\int_0^t C_T(\tau)d\tau}{C_T(t)} = DVR\frac{\int_0^t C_r(\tau)d\tau}{C_T(t)} + B \tag{39}$$

in which $DVR = B_{ND} + 1$ and B is assumed to be constant (when C_T/C_r is constant after some time t*).

5.5.4 Multilinear reference tissue model (MRTM)

In the reference Logan model, it is assumed that C_T/C_r becomes constant after some time. If this is not the case, the Ichise model $MRTM_0$ can be used (Ichise et al. (2003)):

$$\frac{\int_0^t C_T(\tau)d\tau}{C_T(t)} = DVR\frac{\int_0^t C_r(\tau)d\tau}{C_T(t)} + A'\frac{C_r(t)}{C_T(t)} + b \tag{40}$$

in which $DVR = B_{ND} + 1$, $A' = -DVR/k_2'$ and b is assumed to be constant.

This equation can be rearranged in the following form (MRTM):

$$C_T(t) = -\frac{DVR}{b} \int_0^t C_r(s)ds + \frac{1}{b} \int_0^t C_T(s)ds - \frac{DVR}{k_2'b}C_r(t).$$ (41)

The advantage of this expression is that C_T is not present in the independent variables because C_T can be noisy.

Other variants of these models exist in which k_2' is assumed to be known. The difference between these models is mainly based on the strategy to determine k_2'.

5.6 Displacement studies

Displacement studies are important in the validation process of a new tracer. Based on *in vitro* experiments, the affinity for a receptor system can be determined but this doesn't guarantee that the tracer will behave *in vivo* exactly as predicted. By performing an *in vivo* displacement study, the binding to a certain receptor system can be proven. The underlying assumption is that the drug used for the displacement study has a well-characterized affinity for the receptor system under investigation which is higher than the affinity of the tracer itself. If this is not the case, the displacement will be more subtle and may not be detectable.

A displacement study starts with the injected tracer (either as bolus or constant infusion) having reached an equilibrium state. This is disturbed by introducing a nonradioactive competitor which can be either endogenous (e.g. subject performs a cognitive task resulting in neurotransmitter release) or exogenous (e.g. infusion of a drug). The nonradioactive ligand 'displaces' the radioactive one by occupying available receptors hence promoting tracer wash-out (assuming the tracer is not bound irreversibly). The decrease in tracer binding can be detected either by comparing two scans, one with and one without nonradioactive competitor, or by modelling the competition (e.g. Morris and Yoder (2007)).

5.7 Occupancy studies

Occupancy studies are important to test new drugs. Too little occupancy of specific target receptors will not lead to a drug effect while a dose that is much higher than needed to occupy almost all receptors of the target, will not show additional benefits and may cause more negative side-effects than necessary.

Occupancy O of a target receptor system by a drug is defined as:

$$O(t) = 100.\frac{V_T(0) - V_T(t)}{V_T(0) - V_{ND}}$$ (42)

in which $V_T(0)$ is the volume of distribution at baseline (i.e. no drug is given), $V_T(t)$ is the volume of distribution at time t after drug intake and V_{ND} is the volume of distribution of the non-displaceable part of the tracer, i.e. the free and non-specifically bound tracer (e.g. as measured in a reference region where the target receptor is absent). Note that the occupancy is expressed in % and that it is time-dependent. It can also vary across different parts of the brain.

Unlike displacement studies, occupancy studies start with a certain equilibrium level of cold ligand (the drug of interest) present, followed by injection of the tracer to estimate the

remaining fraction of available receptors not bound by the drug. In addition to one baseline scan in the absence of the drug, this typically requires multiple scans at different time points. These time points depend on the kinetics of the drug under investigation. The number of time points is limited by constraints on the amount of blood that can be sampled (if applicable) and on the radiation exposure to the subject. Therefore, occupancy studies are often first performed in monkeys in which at least the constraint on the radiation exposure is weaker compared to humans. In such a case, the occupancy is expressed as function of the plasma concentration of the drug and this relationship is usually modelled with a Hill function. Based on these animal data and on plasma kinetics data in humans, a few time points can be selected to determine the occupancy in-vivo in humans.

5.8 Optimization procedures

The model estimate $\hat{y}_i$ of the PET measurement y_i of frame i is given by:

$$\hat{y}_i = \frac{\int_{t_i^b}^{t_i^e} \{(1 - V_b)C_T(s) + V_bC_a(s)\}ds}{t_i^e - t_i^b} \tag{43}$$

in which t_i^b and t_i^e are the begin time respectively end time of frame i. V_b is the fraction of blood in the volume of interest which can be fitted or fixed to some value. If we have an appropriate sampling scheme, we can approximate M_i by

$$\hat{y}_i = (1 - V_b)C_T(t_i) + V_bC_a(t_i) \tag{44}$$

where the midscan time of frame i is given by $t_i = (t_i^e - t_i^b)/2$.

The cost function O that is used very often, is then defined as:

$$O = \sum_{i=1}^{N} w_i(y_i - \hat{y}_i)^2 \tag{45}$$

in which N is the number of frames, w_i is the weigth of frame i, and $\hat{y}_i$ is the model estimate of observation y_i. The weight is typically inversely proportional to the variance σ_i^2 in frame i:

$$w_i = \frac{1}{\sigma_i^2}. \tag{46}$$

Several models for the variance can be used: e.g. a uniform variance model, a model taking into account the decay correction factors or a model based on the length of the frame, the number of trues and the decay factor that is used. Each of these models will introduce some bias compared to the true variance which is very difficult to determine (Yaqub et al. (2006)). Weights are normalized so that they sum to 1. A priori it is not easy to determine which weighting scheme is the most appropriate but often a uniform weighting scheme is used.

In some models (e.g. reference Logan), we assume that $\hat{y}_i = C_T(t_i)$.

Every model contains one or more parameters which have to be estimated. In some cases parameters can be calculated based on a linear regression but often it is necessary to use non-linear estimation methods. Furthermore, many parameters of interest are by definition positive and it can be useful to constrain the solution to a physiologically acceptable range.

A major problem when using non-linear estimation methods, is that they are time consuming and depend on the initial values that have to be set. In a high-dimensional space (in which each dimension represents a parameter that has to be fitted) with noisy data, the cost function has many local minima. Depending on the initial condition and on the mathematical algorithm that is used, the result of the optimization problem is a local minimum that unfortunately need not to be the global minimum. If we use global optimization algorithms like simulated annealing, we will in theory find the global minimum but the time to find the solution is much longer compared to the other optimization algorithms.

In addition to the presence of local minima, other factors affecting the accuracy of the solution are the initial values if needed, the noise in the data, and the correlation that may be present among different variables.

A summary of the main points to consider for kinetic modelling is given in table 4.

Models
compartmental models
number of compartments
interpretation of compartments
reversible or irreversible binding
parameters of interest
graphical models (linearization)
choice of model
assumptions
if needed, start time for linearization (t^*)
reference models
compartmental or graphical model
choice of reference region
assumptions regarding reference region tracer kinetics
Displacement studies
assumptions about competitor drug's kinetics and affinity
compare 2 scans or model competition
Occupancy studies
assumptions about inital cold ligand's kinetics and affinity
selected time points for scans (e.g. based on animal studies)
Optimization
cost function
initial values
constrain solution to physiologically acceptable range
mathematical algorithm for optimization
Volume of interest or voxel-based approach
size of the smoothing kernel reflecting expected effect size (voxel-based)
processing time
VOI definition
error estimates (voxel-based)

Table 4. Main points to consider for kinetic modelling

6. Model selection

When comparing models or when looking for the best model, the problem of a gold standard arises. Often, a two-tissue compartment model with a measured input function is considered the "best" model. Although this might theoretically be one of the best models, in practice this model is sensitive to all kinds of errors (movement of the patient, errors in timing, errors in determining the input function, etc). This is of course true for other methods as well but simplified models tend to be more robust. One way to solve this, is to use more realistic simulations to study the sensitivity of models to this type of error. Furthermore, when real measurements are used, a strict quality assurance protocol should be in place to evaluate the quality of all data and to minimize errors.

Despite this, comparing different models is complex. Models with more parameters tend to more accurately describe the data. Let P be the number of parameters in the model, N the number of observations and SS the residual sum of squares given by:

$$SS = \sum_{i=1}^{N} w_i (y_i - \hat{y}_i)^2 \tag{47}$$

in which w_i is the weight of observation i, y_i is the i-th observation and $\hat{y}_i$ is the model estimate of observation i.

Several measures exist to help in model selection, the two most popular ones being the Akaiki and the Schwarz criteria:

1. The Akaike information criterion AIC is defined as in Turkheimer et al. (2003):

$$AIC = N \ln(\frac{SS}{N}) + 2P. \tag{48}$$

   Usually, N is not large enough compared to P (i.e. $\frac{N}{P} < 40$) and in such a case we have to use an expression with a correction term (Turkheimer et al. (2003)):

$$AIC_{cor} = N \ln(\frac{SS}{N}) + 2P + \frac{2P(P+1)}{N-P-1}. \tag{49}$$

2. Another criterion that is used sometimes, is the Schwarz criterion given by:

$$SC = N \ln(\frac{SS}{N}) + P \ln(N). \tag{50}$$

In both cases, the model with the lowest value is the most appropriate.

To study the agreement between two different models (or a model and the gold standard), a Bland-Altman plot can be used. This is a plot in which the difference between two model parameters is plotted as function of the average value. It offers a better way of assessing the agreement between two different methods than plotting a correlation between the two different methods since a correlation can simply be high when there is a lot of variability within each method.
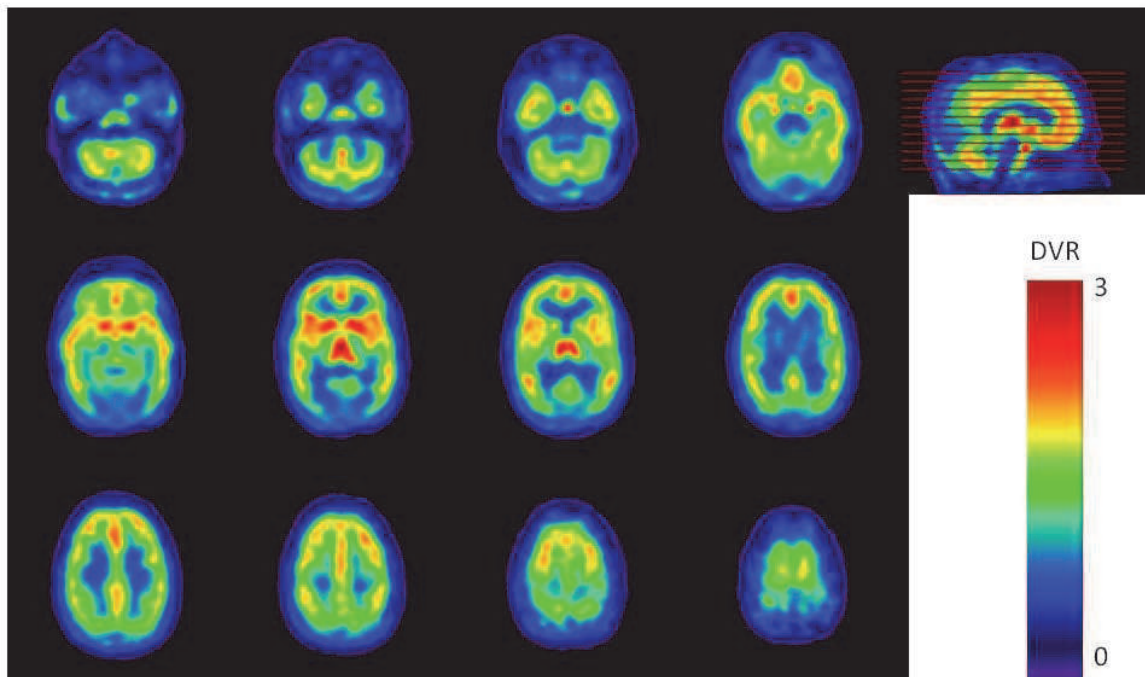
Fig. 9. Parametric image of DVR when using the tracer $[^{11}C]$-Carfentanil to measure opioid receptors

7. Parametric imaging

In traditional parametric image analysis, a kinetic model is performed in each (brain) voxel independently. In contrast, VOI based analysis is spatially biased due to the observer drawing VOIs or at least selecting usually anatomical areas to include in each VOI. Since there is no averaging of the signal over multiple voxels (and potentially large areas), voxel-based analysis is more sensitive than VOI based approaches to pick up small localised changes, but also to noise that will propagate throughout the analysis. As a trade-off, some spatial sensitivity is sacrificed to reduce the effect of noise in the input data (frames of raw counts) by smoothing the data prior to kinetic modelling, e.g. with a Gaussian kernel with a small full width at half maximum (FWHM) such as 6 mm.

Partial volume correction can be performed in a voxel-wise manner as well, by segmenting a coregistered anatomical MRI image into grey matter, white matter and cerebrospinal fluid. The effects of misregistrations and inaccurate segmentations are more likely to impact voxel-wise analyses whereas they may average out in VOI-based analyses.

The resulting output will be parametric images of the kinetic modelling parameters, such as k3 or DVR (figure 9), which can then be entered into voxel-wise statistical analyses after being spatially warped into a common stereotactic (e.g. MNI) space and another smoothing operation is performed. This pre-analysis smoothing serves to correct for remaining inaccuracies in spatial normalisation and normal intersubject variability, but also to ensure assumptions are met for voxel-wise parametric statistics (more specifically, its correction for multiple comparisons by means of Gaussian random field theory). In general, the size of the smoothing kernel determines the size of the effects the analysis is most sensitive to. Smoothing kernels around 10 mm FWHM are commonly used.

8. Future developments

A great challenge is to apply kinetic modelling in small animal brain imaging. Small animal imaging using dedicated PET systems has its own problems and limitations and although theoretically most of what is described in this chapter could be used, in practice it is generally not possible. For a review on kinetic modelling in small animal imaging with PET, the reader is referred to Dupont and Warwick (2009).

A new development is the use of PET to detect endogenous releases of neurotransmitters using a stimulation paradigm. This is a great challenge since the signal changes are very weak. Therefore, simulations are needed first to quantify the effect of different stimulus paradigms and to estimate signal changes (Muylle et al. (2008)).

In this chapter we have looked at relatively simple models described by first order differential equations in which the rate constants were time-independent. More complex models are developed however models with too many parameters are not suitable for use in PET imaging. On the other hand, simple measures like standard uptake value (SUV) or a simple ratio can be investigated in different pathological conditions and compared with parameters derived from kinetic modelling as described in this chapter. These very simple measures clearly have several drawbacks and should be used with care, but they are easy to determine, which is important when using them in a clinical setting.

9. References

Backes, H.; Ullrich, R.; Neumaier, B.; Kracht, L.; Wienhard, K. & Jacobs, A.H. (2009). Noninvasive quantification of 18F-FLT human brain PET for the assessment of tumour proliferation in patients with high-grade glioma, *European Journal of Nuclear Medicine and Molecular Imaging* Vol. 36: 1960-7.

Baete, K.; Nuyts, J.; Van Laere, K.; Van Paesschen, W.; Ceyssens, S.; De Ceuninck, L.; Gheysens, O.; Kelles, A.; Van den Eynden, J.; Suetens, P. & Dupont, P. (2004). Evaluation of Anatomy Based Reconstruction for Partial Volume Correction in Brain FDG-PET, *NeuroImage* Vol. 23: 305-317.

Belanger, M.J.; Mann, J.J. & Parsey, R.V. (2004). OS-EM and FBP reconstructions at low count rates: effect on 3D PET studies of [11C] WAY-100635, *NeuroImage* Vol. 21: 244-50.

Boellaard, R.; van Lingen, A. & Lammertsma, A.A. (2001). Experimental and clinical evaluation of iterative reconstruction (OSEM) in dynamic PET: quantitative characteristics and effects on kinetic modeling, *Journal of Nuclear Medicine* Vol. 42: 808-17.

Catana, C.; Benner, T.; van der Kouwe, A.; Byars, L.; Hamm, M.; Chonde, D.B.; Michel, C.J.; El Fakhri, G.; Schmand, M. & Sorensen, A.G. (2011). MRI-assisted PET motion correction for neurologic studies in an integrated MR-PET scanner, *Journal of Nuclear Medicine* Vol. 52: 154-61.

Carson, R.E. (2000). PET physiological measurements using constant infusion, *Nuclear Medicine and Biology* Vol. 27: 657-60.

Chen, K.; Bandy, D.; Reiman, E.; Huang, S.C.; Lawson, M.; Feng, D.; Yun, L.S. & Palant, A.J. (1998). Noninvasive quantification of the cerebral metabolic rate for glucose using positron emission tomography, 18F-fluoro-2-deoxyglucose, the Patlak method, and an image-derived input function, *Journal of Cerebral Blood Flow & Metabolism* Vol. 18: 716-23.

Croteau, E.; Lavallée, E.; Labbe, S.M.; Hubert, L.; Pifferi, F.; Rousseau, J.A.; Cunnane, S.C.; Carpentier, A.C.; Lecomte, R. & Bénard, F. (2010). Image-derived input function in dynamic human PET/CT: methodology and validation with 11C-acetate and 18F-fluorothioheptadecanoic acid in muscle and 18F-fluorodeoxyglucose in brain, *European Journal of Nuclear Medicine and Molecular Imaging* Vol. 37: 1539-50.

De Man, B.; Nuyts, J.; Dupont, P.; Marchal, G. & Suetens, P. (2000). Reduction of metal streak artifacts in x-ray computed tomography using a transmission maximum a posteriori algorithm, *IEEE Transactions on Nuclear Science* Vol. 47: 977-981

Dupont, P. & Warwick, J. (2009). Kinetic modeling in small animal imaging with PET, *Methods* Vol. 48: 98-103.

Hapdey, S.; Buvat, I.; Carson, J.M.; Carrasquillo, J.A.; Whatley, M. & Bacharach, S.L. (2011). Searching for alternatives to full kinetic analysis in 18F-FDG PET: an extension of the simplified kinetic analysis method, *Journal of Nuclear Medicine* Vol. 52: 634-41.

Hunter, G.J.; Hamberg, L.M.; Alpert, N.M.; Choi, N.C. & Fischman, A.J. (1996). Simplified measurement of deoxyglucose utilization rate, *Journal of Nuclear Medicine* Vol. 37: 950-5.

Ichise, M.; Liow, J.S.; Lu, J.Q.; Takano, A.; Model, K.; Toyama, H.; Suhara, T.; Suzuki, K.; Innis, R.B. & Carson, R.E. (2003). Linearized reference tissue parametric imaging methods: application to [11C]DASB positron emission tomography studies of the serotonin transporter in human brain, *Journal of Cerebral Blood Flow & Metabolism* Vol. 23: 1096-112.

Innis, R.B.; Cunningham, V.J.; Delforge, J.; Fujita, M.; Gjedde, A.; Gunn, R.N.; Holden, J.; Houle, S.; Huang, S.C.; Ichise, M.; Iida, H.; Ito, H.; Kimura, Y.; Koeppe, R.A.; Knudsen, G.M.; Knuuti, J.; Lammertsma, A.A.; Laruelle, M.; Logan, J.; Maguire, R.P.; Mintun, M.A.; Morris, E.D.; Parsey, R.; Price, J.C.; Slifstein, M.; Sossi, V.; Suhara, T.; Votaw, J.R.; Wong, D.F. & Carson, R.E. (2007). Consensus nomenclature for in vivo imaging of reversibly binding radioligands, *Journal of Cerebral Blood Flow & Metabolism* Vol. 27: 1533-9.

Lammertsma, A.A. & Hume, S.P. (1996). Simplified reference tissue model for PET receptor studies, *NeuroImage* Vol. 4: 153-8.

Lammertsma, A.A.; Bench, C.J.; Hume, S.P.; Osman, S.; Gunn, K.; Brooks, D.J. & Frackowiak, R.S. (1996). Comparison of methods for analysis of clinical [11C]raclopride studies, *Journal of Cerebral Blood Flow & Metabolism* Vol. 16: 42-52.

Lemmens, C.; Montandon, ML.; Nuyts, J.; Ratib, O.; Dupont, P. & Zaidi, H. (2008). Impact of metal artifacts due to EEG electrodes in brain PET/CT Imaging, *Physics in Medicine and Biology*, Vol. 53: 4417-4429.

Logan, J.; Fowler, J.S.; Volkow, N.D.; Wang, G.J.; Ding, Y.S.& Alexoff, D.L. (1996). Distribution volume ratios without blood sampling from graphical analysis of PET data, *Journal of Cerebral Blood Flow & Metabolism* Vol. 16: 834-40.

Maguire, R.P.; Calonder, C. & Leenders, K.L. (1996). Patlak Analysis applied to Sinogram Data in Myers, R.; Cunningham, V.; Bailey, D. & Jones T. (Eds.), *Quantification of Brain Function Using PET*, Academic Press, New York, pp. 307-311.

Montgomery, A.J.; Thielemans, K.; Mehta, M.A.; Turkheimer, F.; Mustafovic, S. & Grasby, P.M. (2006). Correction of head movement on PET studies: comparison of methods, *Journal of Nuclear Medicine* Vol. 47: 1936-44.

Morimoto, T.; Ito, H.; Takano, A.; Ikoma, Y.; Seki, C.; Okauchi, T.; Tanimoto, K.; Ando, A.; Shiraishi, T.; Yamaya, T. & Suhara, T. (2006). Effects of image reconstruction

algorithm on neurotransmission PET studies in humans: comparison between filtered backprojection and ordered subsets expectation maximization, *Annals of Nuclear Medicine* Vol. 20: 237-43.

Morris, E.D. & Yoder, K.K. (2007). Positron emission tomography displacement sensitivity: predicting binding potential change for positron emission tomography tracers based on their kinetic characteristics, *Journal of Cerebral Blood Flow & Metabolism* Vol. 27: 606-17.

Mourik, J.E.; van Velden, F.H.; Lubberink, M.; Kloet, R.W.; van Berckel, B.N.; Lammertsma, A.A. & Boellaard, R. (2008). Image derived input functions for dynamic High Resolution Research Tomograph PET brain studies, *NeuroImage* Vol. 43: 676-86.

Müller-Gärtner, H.W.; Links, J.M.; Prince, J.L.; Bryan, R.N.; McVeigh, E.; Leal, J.P.; Davatzikos, C. & Frost, J.J. (1992). Measurement of radiotracer concentration in brain gray matter using positron emission tomography: MRI-based correction for partial volume effects, *Journal of Cerebral Blood Flow & Metabolism* Vol. 12: 571-83.

Muylle, T.; Dupont, P. & Van Laere, K. (2008). On the detection of endogenous ligand release with PET: A simulation study, *NeuroImage* Vol. 41: T75.

Naganawa, M.; Kimura, Y.; Ishii, K.; Oda, K.; Ishiwata, K. & Matani, A. (2005). Extraction of a plasma time-activity curve from dynamic brain PET images based on independent component analysis, *IEEE Transactions on Biomedical Engineering* Vol. 52: 201-210.

Oda, K.; Toyama, H.; Uemura, K.; Ikoma, Y.; Kimura, Y. & Senda, M. (2001). Comparison of parametric FBP and OS-EM reconstruction algorithm images for PET dynamic study, *Annals of Nuclear Medicine* Vol. 15: 417-23.

Rahmim, A.; Tang, J. & Zaidi, H. (2009). Four-dimensional (4D) image reconstruction strategies in dynamic PET: beyond conventional independent frame reconstruction, *Medical Physics* Vol. 36: 3654-70.

Reilhac, A.; Tomei, S.; Buvat, I.; Michel, C.; Keheren, F. & Costes, N. (2008). Simulation-based evaluation of OSEM iterative reconstruction methods in dynamic brain PET studies, *NeuroImage* Vol. 39: 359-68.

Turkheimer, F.E.; Hinz, R. & Cunningham, V.J. (2003). On the Undecidability Among Kinetic Models: From Model Selection to Model Averaging, *Journal of Cerebral Blood Flow & Metabolism*, Vol. 23: 490-498.

Walker, M.D.; Asselin, M.C.; Julyan, P.J.; Feldmann, M.; Talbot, P.S.; Jones, T. & Matthews, J.C. (2011). Bias in iterative reconstruction of low-statistics PET data: benefits of a resolution model, *Physics in Medicine and Biology* Vol. 56: 931-49.

Wang, G.; Fu, L. & Qi, J. (2008). Maximum a posteriori reconstruction of the Patlak parametric image from sinograms in dynamic PET, *Physics in Medicine and Biology* Vol. 53: 593-604.

Wang, G. & Qi, J. (2009). Generalized algorithms for direct reconstruction of parametric images from dynamic PET data, *IEEE Transactions on Medical Imaging* Vol. 28: 1717-26.

Yaqub, M.; Boellaard, R.; Kropholler, M.A. & Lammertsma, A.A. (2006). Optimization algorithms and weighting factors for analysis of dynamic PET studies, *Physics in Medicine and Biology* Vol. 51: 4217-32.

Zanotti-Fregonara, P.; Liow, J.S.; Fujita, M.; Dusch, E.; Zoghbi, S.S.; Luong, E.; Boellaard, R.; Pike, V.W.; Comtat, C. & Innis, R.B. (2011). Image-derived input function for human brain using high resolution PET imaging with [C](R)-rolipram and [C]PBR28, *PLoS ONE* Vol. 25: e17056.
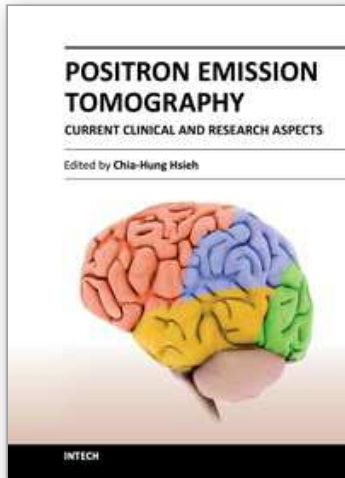
Positron Emission Tomography - Current Clinical and Research Aspects

Edited by Dr. Chia-Hung Hsieh

This book's stated purpose is to provide a discussion of the technical basis and clinical applications of positron emission tomography (PET), as well as their recent progress in nuclear medicine. It also summarizes current literature about research and clinical science in PET. The book is divided into two broad sections: basic science and clinical science. The basic science section examines PET imaging processing, kinetic modeling, free software, and radiopharmaceuticals. The clinical science section demonstrates various clinical applications and diagnoses. The text is intended not only for scientists, but also for all clinicians seeking recent information regarding PET.

How to reference

In order to correctly reference this scholarly work, feel free to copy and paste the following:

Natalie Nelissen, JamesWarwick and Patrick Dupont (2012). Kinetic Modelling in Human Brain Imaging, Positron Emission Tomography - Current Clinical and Research Aspects, Dr. Chia-Hung Hsieh (Ed.), ISBN: 978-953-307-824-3, InTech, Available from: http://www.intechopen.com/books/positron-emission-tomography-current-clinical-and-research-aspects/kinetic-modelling-in-human-brain-imaging

INTECH
open science | open minds